ENGINEERING Information Technology & Electronic Engineering
https://www.academax.com/EITEE; https://www.engineering.org.cn
https://ieeexplore.ieee.org/xpl/RecentIssue.jsp?punumber=11344065
E-mail: eng.itee@zju.edu.cn

Engineering Journals
Available on IEEE Xplore®

Correspondence

https://doi.org/10.1631/ENG.ITEE.2025.0023

Miniaturized bandpass filter with a wide upper stopband using isomeric resonators in a cavity

Chengyang ZHANG[1], Ying XUE[1], Qingyuan LU[2], Jianxin CHEN[1]✉

[1]*School of Information Science and Technology, Nantong University, Nantong 226019, China*
[2]*Xinglin College, Nantong University, Nantong 226019, China*

1 Introduction

Recently, the increasing demand for advanced telecommunication systems has spurred extensive research into bandpass filters (BPFs), with particular emphasis on miniaturization, reduction of insertion loss (IL), and enhancement of upper stopband rejection (Huang et al., 2021; Snyder et al., 2021; Lin et al., 2023; Zeng et al., 2023).

The metal waveguide (WG) filter has been the subject of extensive research due to its high power capacity and low loss (Wong et al., 2021; Xiang et al., 2023). However, the substantial size of filter circuitry poses significant challenges to the miniaturization required in modern communication systems (Fang et al., 2022). Dielectric resonator (DR)-loaded cavities (Chen et al., 2016; Tomassoni et al., 2016; Widaa and Höft, 2023) and dielectric WGs (Xie et al., 2023; Qin et al., 2024; Tang et al., 2024; Xu et al., 2024) are widely employed to reduce dimensions. Nevertheless, spurious responses associated with either DR-loaded cavities or dielectric WGs persist, leading to insufficient suppression of the upper stopband and limiting their application in multi-standard wireless communication systems (Zhao et al., 2022).

Relatively speaking, ridge WG technology has attracted increasing attention because of its potential for size reduction and improved upper stopband performance (Fahmi et al., 2009; di Crestvolant and de Paolis, 2018; Chen et al., 2024; Zhang et al., 2025). Recently, a U-shaped ridge resonator was proposed to generate a transmission zero (TZ) either above or below the passband (Chaudhary and Ahmed, 2023). However, the upper stopband performance and overall size of the cavity BPF were not addressed. To reduce the filter length, the coupling structure between ridge WG resonators was modified to width-reduced rectangular WGs (Chen et al., 2025). This modification shortens the distance between ridge WG resonators and introduces TZs. Nevertheless, the filter length remains relatively large due to cascade coupling of the ridge WG resonators, and the improvement in upper stopband performance is limited. Moreover, the TZ in the upper stopband cannot be independently controlled because the coupling between the first and third resonators, K_{13}, is determined once the coupling between the first and second resonators, K_{12}, is established in traditional inline cavity BPFs.

In this paper, based on the E-field distributions of the first two modes in ridge WG resonators (TE_{101} and TE_{102} modes), a tuning post (Tup) is embedded in the central region of the ridge. By adjusting the Tup depth, the resonant frequency of the fundamental TE_{101} mode (f_{101}) is significantly reduced, whereas the first harmonic TE_{102} mode remains almost unchanged, indicating that both miniaturization and a wide upper stopband can be achieved. Furthermore, a half-wavelength resonant slot (HWRS) resonator is introduced between two ridge WG resonators to construct a three-pole BPF. This configuration reduces the BPF length and introduces cross-coupling, thereby generating a TZ in the upper stopband. In addition, the thickness of the HWRS resonator provides an extra path to control the cross-coupling, enabling precise TZ positioning within a certain range. Measurement results indicate that the proposed filter achieves a size reduction of approximately 90% and wider upper stopband rejection compared with a filter based on a traditional ridge WG (Chen et al., 2025).

2 General structure and design

The proposed BPF is a three-pole filter using isomeric resonators in a cavity, consisting of two ridge WG resonators and an HWRS in between. As illustrated in Fig. 1, the ridges are designed to be reentrant to allow the embedding of the Tup.

2.1 Working principle of the ridge WG resonator with Tup

As illustrated in Fig. 2a, a metal ridge (a_r×b_r=10 mm×11.8 mm) is inserted into an evanescent-mode rectangular WG (a×b=25.2 mm×12.6 mm) to form a ridge WG resonator. The first two modes of the

✉ Jianxin CHEN, jjxchen@hotmail.com
Chengyang ZHANG, https://orcid.org/0009-0000-4173-341X
Jianxin CHEN, https://orcid.org/0000-0002-8703-5294
CLC number: TN015

Received: Sept. 8, 2025; Revision accepted: Jan. 6, 2026;
Crosschecked: Jan. 16, 2026

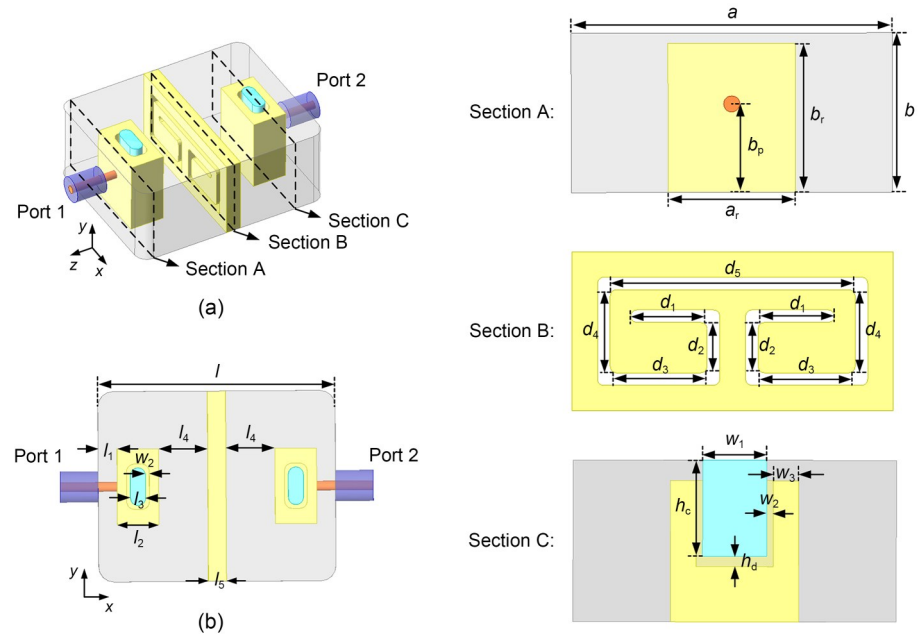

Fig. 1 The 3D view (a) and top view (b) of the configuration of the proposed filter. Parameters are a=25.2, b=12.6, a_r=10, b_r=11.8, b_p=7, d_1=6, d_2=4, d_3=7.6, d_4=6.6, d_5=19.2, h_c=7.5, w_1=5, w_2=0.5, w_3=0.5, h_d=0.8, l=32.8, l_1=2.5, l_2=5.5, l_3=2, l_4=7.1, and l_5=2.6 (unit: mm)

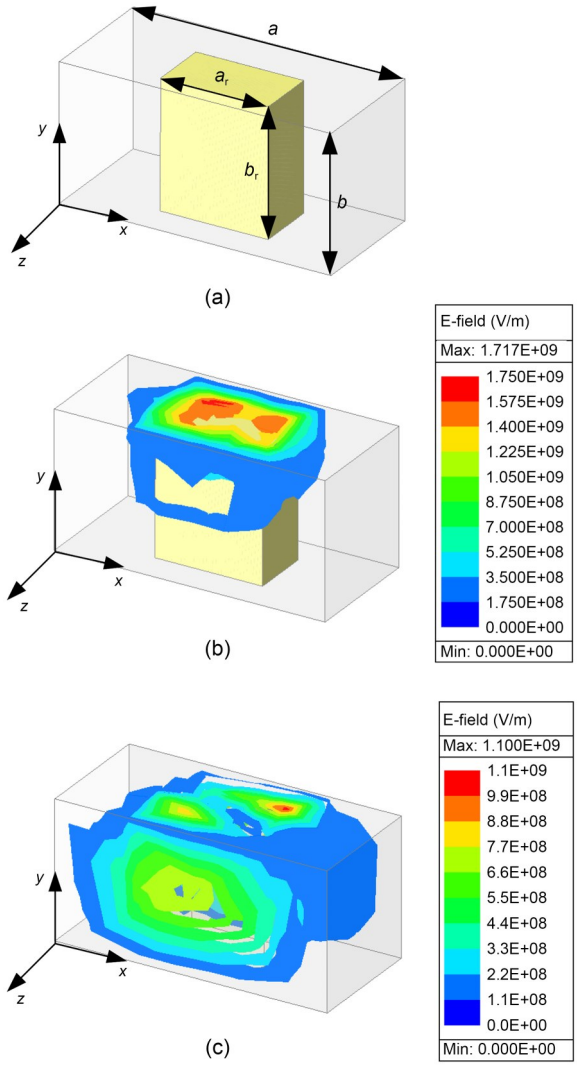

Fig. 2 Ridge waveguide resonator (a) and the E-field distributions of TE_{101} (b) and TE_{102} (c) modes

ridge WG resonator are the TE_{101} and TE_{102} modes, as shown in Fig. 2. The E-field of the TE_{101} mode is predominantly concentrated in the central region above the ridge, whereas that of the TE_{102} mode is distributed in the longitudinal regions above the ridge. Therefore, the Tup can be strategically embedded in the central region of the ridge, as shown in Fig. 3a, to modulate f_{101}.

As shown in Fig. 3b, the modulation range of f_{101} is approximately 0%–45%, which can be combined with the analysis of ridged WG modes to predict f_{101} (Utsumi, 1985). Meanwhile, f_{102} remains almost constant as the height of the Tup (h_c) increases, whereas f_{101} exhibits a decreasing trend with increasing h_c or w_1, as shown in Figs. 3b and 3c. In addition, the unloaded quality factor Q_u of the TE_{101} mode decreases, as shown in Fig. 3d. These results indicate that the introduction of the Tup can reduce f_{101} while forming a wide spurious-free range between the two modes. As illustrated in Fig. 4(a), the first higher-order resonant frequency f_1 of the ridge WG resonator with Tup decreases as h_c increases or w_1 decreases. Concurrently, f_{101} also varies with changes in h_c or w_1, resulting in an expanded single-mode operating bandwidth n (n=f_1/f_{101}), which increases as h_c or w_1 increases, as shown in Fig. 4b.

According to Fig. 3d and Fig. 4, a compromise is required among Q_u, size reduction, and spurious range. To maintain a Q_u value exceeding 1300, the parameters h_c and w_1 are set to 7.5 mm and 5 mm, respectively.

2.2 Resonant coupling structure

As shown in Fig. 5a, the proposed resonant coupling structure is formed by an HWRS resonator. As shown in Fig. 5b, the resonant frequency of the proposed resonant coupling structure (f_{s0}) is primarily determined by the total slot length (d_0=$2d_1$+$2d_2$+$2d_3$+$2d_4$+d_5), following the approximate relationship f_{s0}≈$c/(2d_0)$, where c is the speed of light in vacuum.

Although f_{s0} slightly decreases as the thickness (l_5) increases, it can be decoupled by slightly adjusting d_0. The E-field direction

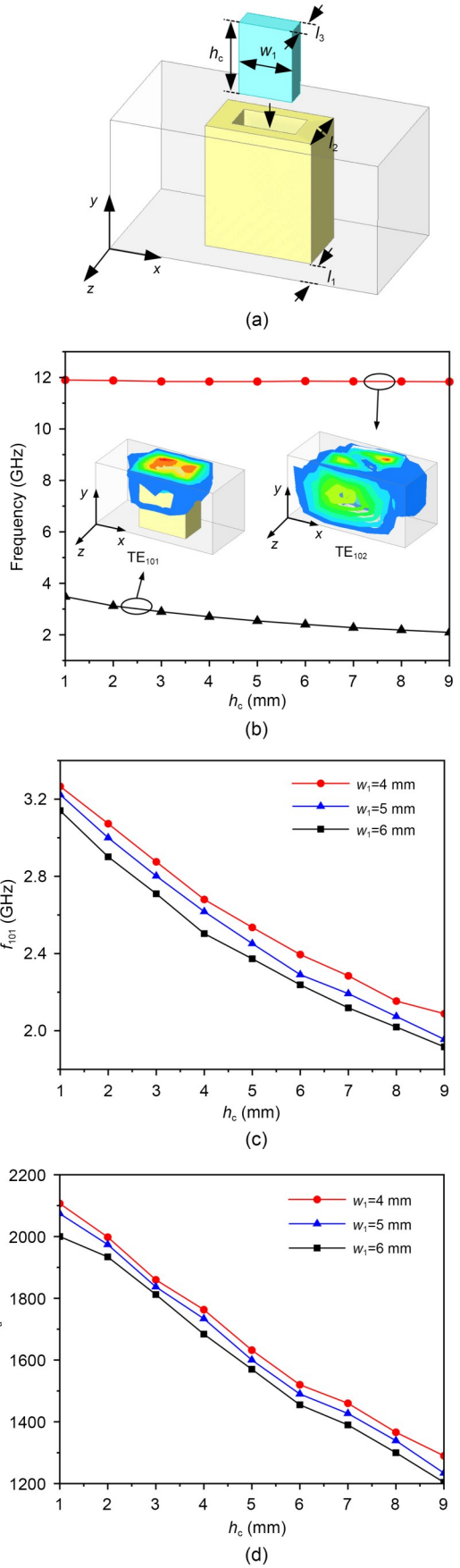

Fig. 3 Ridge waveguide (WG) resonator with Tup (a) (w_1=5, l_1=2.5, l_2=5.5, and l_3=2, in mm), simulated resonant frequency of the ridge WG resonator versus h_c with different modes (TE_{101} and TE_{102} modes) (b), and simulated f_{101} (c) and Q_u (d) versus h_c with different w_1

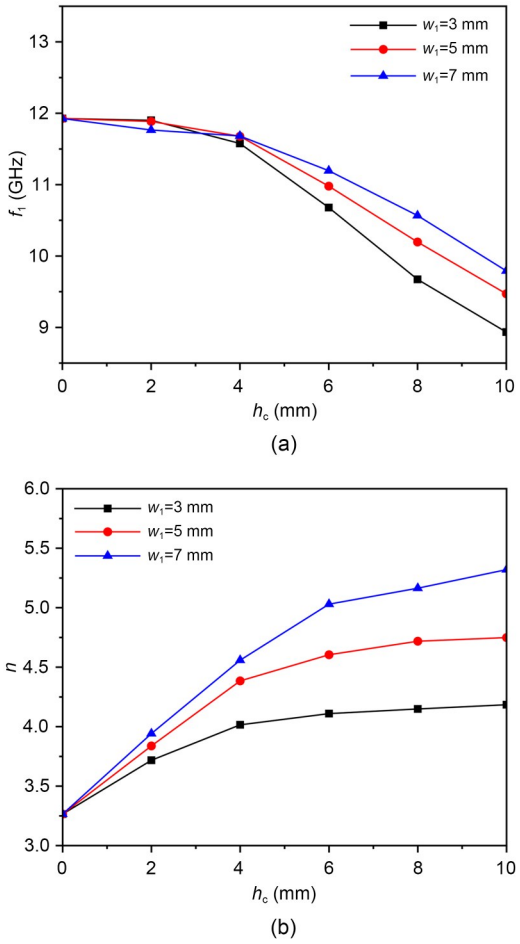

Fig. 4 Simulated f_1 (a) and n (b) versus h_c with different w_1 (n=f_1/f_{101}) (l_1= 2.5 mm, l_2=5.5 mm, and l_3=2 mm)

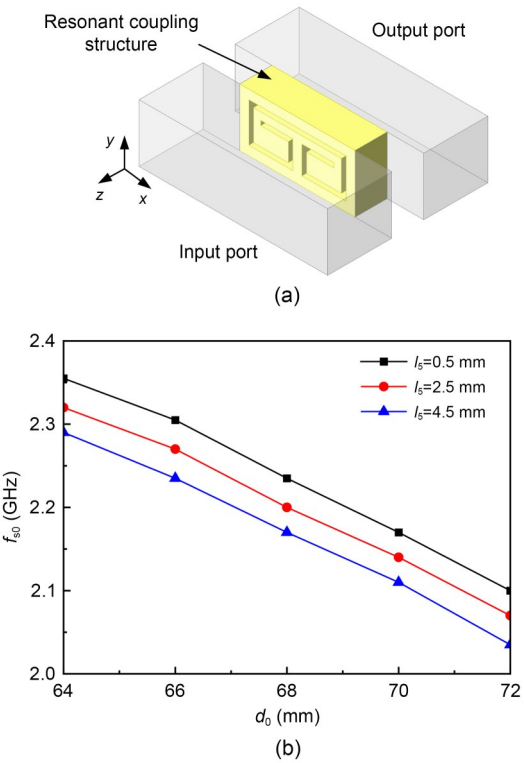

Fig. 5 Proposed resonant coupling structure (a) and f_{s0} versus d_0 with different l_5 (b)

of the resonant coupling structure is shown in Fig. 6. It can be observed that the input and output couplings of the proposed structure have the same E-field direction, implying that the structure can provide the required characteristics to achieve a controllable TZ in the upper stopband.

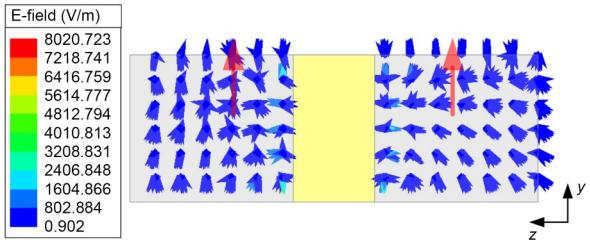

Fig. 6 E-field distribution of the resonant coupling structure

2.3 Design of the compact BPF

Due to the characteristics of the resonant coupling structure, its resonant frequency depends on both l_5 and d_0, implying that, under the condition of meeting the required coupling coefficient, the resonant coupling structure can be designed to be extremely thin. Consequently, the ridge WG resonators are closely arranged in the BPF design. The topology structure of the BPF is shown in Fig. 7.

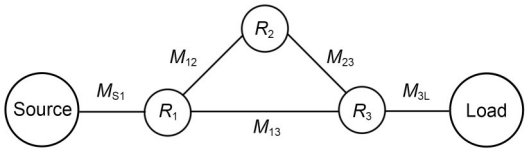

Fig. 7 Coupling topology structure of the proposed bandpass filter

In addition, the ridge WG resonator exhibits a wide single-mode operating bandwidth, within which only the fundamental mode is supported and no higher-order modes are excited. As a result, a broad attenuation region is formed prior to the onset of the first higher-order resonance. As shown in Fig. 8, this attenuation region fully covers the first higher-order mode of the half-mode resonator, indicating that filters employing the isomeric ridge WG and HWRS resonators can realize a wide upper stopband.

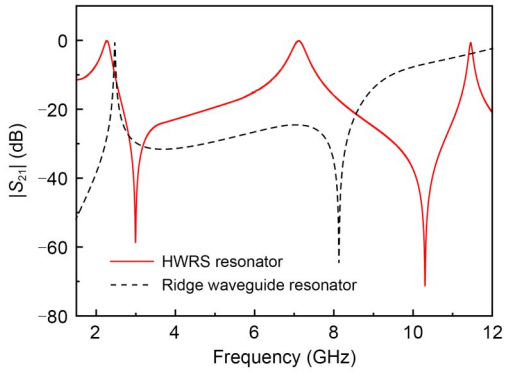

Fig. 8 Simulated $|S_{21}|$ of the HWRS and ridge waveguide resonators

The proposed BPF has a center frequency (f_0) of 2.2 GHz with a 0.3 dB ripple fractional bandwidth of 13%. According to the specifications, the lumped-element values of the low-pass prototype filter are g_0=1, g_1=1.04, and g_2=1.15.

Accordingly, the required external quality factor and coupling coefficients of the BPF are obtained (Hong et al., 2001): Q_e=7.5 and K_{12}=K_{23}=0.12. The coupling matrix is as follows:

$$\begin{bmatrix} 0 & 1.001 & 0 & 0 & 0 \\ 1.001 & 0.093 & 0.867 & 0.405 & 0 \\ 0 & 0.867 & -0.418 & 0.867 & 0 \\ 0 & 0.405 & 0.867 & 0.093 & 1.001 \\ 0 & 0 & 0 & 1.001 & 0 \end{bmatrix}.$$

The extracted Q_e depends on the length l_1 and the height b_p of the feeding probe. As shown in Fig. 9, Q_e increases as b_p increases or l_1 decreases. A parametric investigation of coupling coefficient control is conducted to validate the TZ tuning capability. As illustrated in Figs. 10a and 10b, K_{12} and K_{13} are governed by the distance l_4 between the ridge WG and HWRS resonators. Notably, the thickness l_5 of the HWRS resonator provides an additional control mechanism for K_{13}. From Figs. 10a and 10b, it is evident that K_{13} can be effectively adjusted by varying l_5, whereas K_{12} remains largely unaffected, demonstrating decoupled control capability. Fig. 10c presents the simulation results of BPFs with different l_5. The demonstrated TZ tuning capability enables strategic enhancement of filter upper stopband rejection. After the optimization process, the dimensions of the proposed BPF are provided in the caption of Fig. 1, achieving a size reduction of approximately 90% compared with a filter based on a traditional ridge WG.

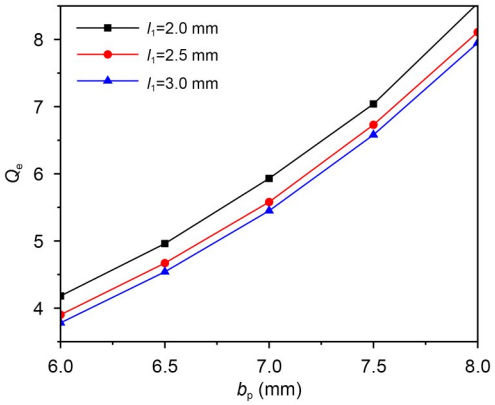

Fig. 9 Extracted Q_e versus b_p with different l_1

3 Simulation and experimental results

Fig. 11 shows a photograph of the fabricated BPF, and the experimental results are measured using an Agilent N5230A PNA-L network analyzer. The measurement and simulation results (Fig. 12) show good agreement. The BPF has f_0=2.2 GHz and a passband ranging from 2.04 to 2.48 GHz, achieving a predefined 3-dB fractional bandwidth of approximately 19%. The measured return loss ($|S_{11}|$) is better than 17 dB, while the minimum IL is 0.45 dB. The proposed design exhibits a wide upper stopband, with a suppression level higher than 30 dB from 2.65 to 10.6 GHz, corresponding to a defined ζ value of 3.63, as listed in Table 1.

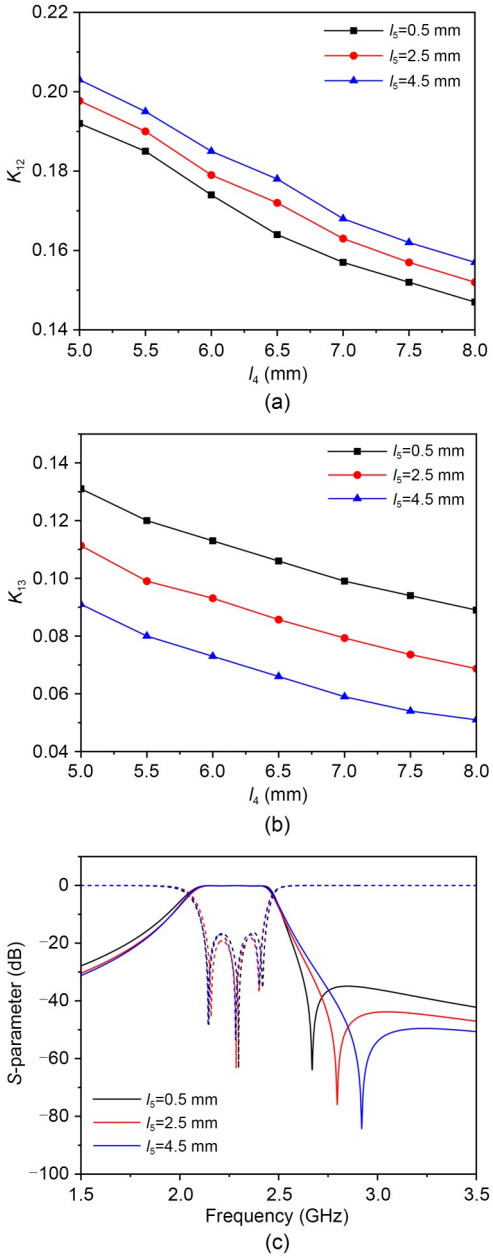

Fig. 10 Extracted K_{12} (a) and K_{13} (b) versus l_4 with different l_5 and simulation results of the proposed bandpass filter with different l_5 (c) (solid lines: $|S_{21}|$; dashed lines: $|S_{11}|$)

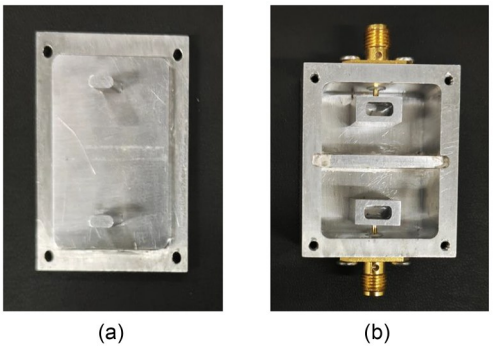

Fig. 11 Top part (a) and bottom part (b) of the prototype

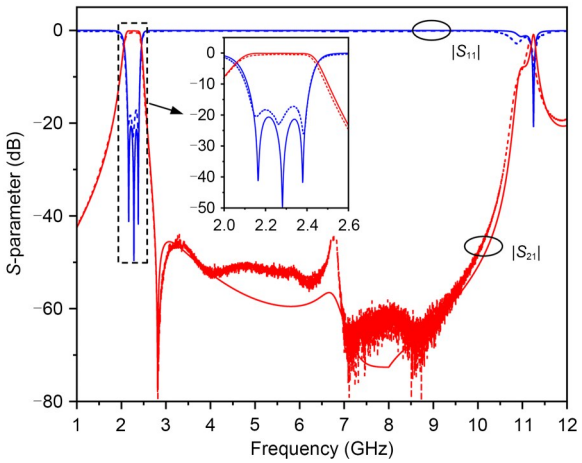

Fig. 12 Simulation (solid lines) and measurement (dashed lines) results

Table 1 summarizes the performance of BPFs using various technologies. As expected, the proposed BPF has the smallest volume ($0.23\lambda_0\times0.18\lambda_0\times0.09\lambda_0$) owing to the use of isomeric resonators in a cavity. It achieves a size reduction of approximately 90% compared with the BPF based on cascade coupling of ridge WG resonators (Chen et al., 2025). Meanwhile, the upper stopband is much wider than those of the designs listed in Table 1 and is comparable to that of a microstrip design with harmonic suppression (Chen et al., 2018), indicating that the proposed design effectively addresses the long-standing issue of harmonic interference in traditional WG filters. In fact, this improved performance is obtained at the expense of passband loss, which is slightly higher than that of WG or ridge WG designs but lower than that of designs based on DRs and dielectric WGs, as listed in Table 1.

4 Conclusions

In this paper, a miniaturized cavity BPF using isomeric resonators is presented, achieving a size reduction of approximately 90%

Table 1 Comparison with other bandpass filters

Reference	Technology	f_0 (GHz)	3-dB fractional bandwidth (%)	Order	Insertion loss (dB)	ζ	3D size (λ_0^3)
Zhu et al. (2024)	Waveguide (WG)	3.72	4.5	3	0.24	0.18	0.72×0.62×0.54
Widaa and Höft (2023)	Dielectric resonator-loaded WG	3.967	0.5	2	1.3	N.A.	0.82×0.26×0.16
Qin et al. (2024)	Dielectric WG	3.45	2.8	3	0.8	1.47	0.34×0.34×0.07
Ruiz-Cruz et al. (2005)	Ridge WG	4	14.6	3	0.3	0.2	0.82×0.33×0.33
Chen et al. (2024)	Ridge WG	3.5	20	3	0.25	1.94	0.44×0.29×0.15
This paper	Ridge WG and resonant slot	2.2	19	3	0.45	3.63	0.23×0.18×0.09

Note: $\zeta=(f_{max}-f_{min})/f_0$, where f_{max} and f_{min} are the maximum and minimum frequencies when $|S_{21}|=-30$ dB in the upper stopband, respectively. λ_0 represents the free space wavelength at f_0

and wider upper stopband rejection compared with a filter based on a traditional ridge WG. The proposed design offers three key advantages: a compact footprint, an extended upper stopband, and a controllable TZ. These features collectively address long-standing challenges in conventional WG filters, including excessive size and harmonic interference, while providing a systematic approach for positioning the TZ within the upper stopband to enhance selectivity. The high performance verified by simulation and experiment makes the proposed filter attractive for practical applications, such as satellite communication.

Acknowledgments

This work was supported by the National Natural Science Foundation of China (No. 62371263) and the Postgraduate Research & Practice Innovation Program of Jiangsu Province (No. SJCK25_1995).

Author contributions

Chengyang ZHANG designed the research, processed the data, and drafted the paper. Jianxin CHEN, Ying XUE, and Qingyuan LU helped organize the paper. Chengyang ZHANG and Jianxin CHEN revised and finalized the paper.

Conflict of interest

All the authors declare that they have no conflict of interest.

Data availability

The data that support the findings of this study are available from the corresponding author upon reasonable request.

Declaration on the use of generative AI tools

During the preparation of this work, the authors used ChatGPT to improve language. After using this tool, the authors reviewed and edited the content as needed and take full responsibility for the content of the published article.

References

Chaudhary MA, Ahmed MM, 2023. Pseudoelliptic waveguide filters using U-shaped ridge resonators. *IEEE Trans Circ Syst II Expr Briefs*, 70(2):371-375. https://doi.org/10.1109/TCSII.2022.3173377

Chen JX, Zhan Y, Qin W, et al., 2016. Analysis and design of balanced dielectric resonator bandpass filters. *IEEE Trans Microw Theory Tech*, 64(5):1476-1483. https://doi.org/10.1109/TMTT.2016.2546260

Chen JX, Li YL, Qin W, et al., 2018. Compact multi-layer bandpass filter with wide stopband using selective feeding scheme. *IEEE Trans Circ Syst II Expr Briefs*, 65(8):1009-1013. https://doi.org/10.1109/TCSII.2017.2782692

Chen JX, Xue Y, Shi X, et al., 2024. Design of double-ridge waveguide balanced filter and filtering power divider. *IEEE Trans Microw Theory Tech*, 72(10):5929-5937. https://doi.org/10.1109/TMTT.2024.3386731

Chen JX, Xue Y, Shi X, et al., 2025. Analysis and design of compact ridge waveguide bandpass filter and filtering balun with improved upper stopband performance. *IEEE Trans Microw Theory Tech*, 73(7):3977-3986. https://doi.org/10.1109/TMTT.2024.3509865

di Crestvolant VT, de Paolis F, 2018. Dimensional synthesis of evanescent-mode ridge waveguide bandpass filters. *IEEE Trans Microw Theory Tech*, 66(2):954-961. https://doi.org/10.1109/TMTT.2017.2750166

Fahmi MM, Ruiz-Cruz JA, Mansour RR, et al., 2009. Compact ridge waveguide filters with arbitrarily placed transmission zeros using nonresonating nodes. *IEEE Trans Microw Theory Tech*, 57(12):3354-3361. https://doi.org/10.1109/TMTT.2009.2034423

Fang X, Li YC, Li LW, et al., 2022. A dual-band tunable balanced filter with independently tuning bands. *IEEE Trans Circ Syst II Expr Briefs*, 69(4):2076-2080. https://doi.org/10.1109/TCSII.2021.3121400

Hong JS, Lancaster MJ, 2001. Microstrip Filters for RF/Microwave Applications. John Wiley & Sons, Inc., New York, NY, USA, p.215-219.

Huang ZY, Jiang Y, Wu WW, et al., 2021. W-band bandpass filter using rectangular micro-coaxial structure. *IEEE Microw Wirel Compon Lett*, 31(8):957-960. https://doi.org/10.1109/LMWC.2021.3092144

Lin JY, Yang Y, Wong SW, et al., 2023. Two-way waveguide diplexer and its application to diplexing in-band full-duplex antenna. *IEEE Trans Microw Theory Tech*, 71(3):1171-1179. https://doi.org/10.1109/TMTT.2022.3218100

Qin W, Zhou YK, Yang WW, et al., 2024. Dielectric waveguide bandpass filters with multiple transmission zeros by constructing cascaded-trisection coupling structures. *IEEE Trans Microw Theory Tech*, 72(7):4218-4228. https://doi.org/10.1109/TMTT.2023.3336282

Ruiz-Cruz JA, Sabbagh MAE, Zaki KA, et al., 2005. Canonical ridge waveguide filters in LTCC or metallic resonators. *IEEE Trans Microw Theory Tech*, 53(1):174-182. https://doi.org/10.1109/TMTT.2004.839324

Snyder RV, Macchiarella G, Bastioli S, et al., 2021. Emerging trends in techniques and technology as applied to filter design. *IEEE J Microw*, 1(1):317-344. https://doi.org/10.1109/JMW.2020.3028643

Tang WS, Li M, Zhang YM, et al., 2024. Compact dielectric waveguide filters with controllable transmission zeros using dual external coupling and hybrid ridge and post. *IEEE Trans Microw Theory Tech*, 72(11):6574-6584. https://doi.org/10.1109/TMTT.2024.3408646

Tomassoni C, Bastioli S, Snyder RV, 2016. Compact mixed-mode filter based on TE_{101} cavity mode and TE_{018} dielectric mode. *IEEE Trans Microw Theory Tech*, 64(12):4434-4443. https://doi.org/10.1109/TMTT.2016.2623714

Utsumi Y, 1985. Variational analysis of ridged waveguide modes. *IEEE Trans Microw Theory Tech*, 33(2):111-120. https://doi.org/10.1109/TMTT.1985.1132958

Widaa A, Höft M, 2023. Widely tunable TM-mode dielectric filters with constant absolute bandwidth using re-entrant caps. *IEEE J Microw*, 3(2):706-714. https://doi.org/10.1109/JMW.2023.3242689

Wong SW, Lin JY, Yang Y, et al., 2021. Waveguide components based on multiple-mode resonators: advances in microwave multiple-mode waveguide components, including multiplexers, three-state diplexers, crossovers, and balanced/unbalanced elements. *IEEE Microw Mag*, 22(2):33-45. https://doi.org/10.1109/MMM.2020.3035863

Xiang KR, Chen FC, Chu QX, 2023. Compact waveguide filters using novel resonant coupling structures. *IEEE Trans Microw Theory Tech*, 71(5):2129-2138. https://doi.org/10.1109/TMTT.2022.3224755

Xie Y, Chen FC, Chu QX, 2023. Inline box-like dielectric filters with asymmetric and symmetric responses. *IEEE Trans Microw Theory Tech*, 71(6):2522-2531. https://doi.org/10.1109/TMTT.2022.3226176

Xu ZY, Wu YL, Li SB, et al., 2024. Exhaustive design and realization for in-line topology quasi-TEM mode dielectric waveguide filter with dispersive couplings. *IEEE Trans Circ Syst II Expr Briefs*, 71(7):3333-3337. https://doi.org/10.1109/TCSII.2024.3364721

Zeng Y, Che C, Yu M, et al., 2023. Novel miniaturized light-weight coaxial cavity filters with electrical mainline couplings. *IEEE J Microw*, 3(3):1040-1050. https://doi.org/10.1109/JMW.2023.3278733

Zhang CY, Shi X, Zhu YH, et al., 2025. A compact interlaced-double-ridge waveguide balanced filter with wideband CM suppression. *IEEE Microw Wirel Technol Lett*, 35(2):169-172. https://doi.org/10.1109/LMWT.2024.3510760

Zhao W, Wu YL, Yang YH, et al., 2022. Novel on-chip wideband filtering power dividers with high selectivity and ultra-wide out-of-band suppression in LTCC technology. *IEEE Trans Circ Syst II Expr Briefs*, 69(11):4288-4292. https://doi.org/10.1109/TCSII.2022.3179308

Zhu YH, Qin W, Chen JX, 2024. Compact waveguide filtering power dividers with flexible division ratio and enhanced selectivity. *IEEE Trans Compon Packag Manuf Technol*, 14(11):2043-2049. https://doi.org/10.1109/TCPMT.2024.3483773